

1
2 **Intraseasonal sea level variability along the western coast of India simulated by an eddy-resolving**
3 **ocean general circulation model**

4
5 **Y. Yamagami¹, T. Suzuki¹, H. Tatebe¹**

6 ¹ Japan Agency for Marine-Earth Science and Technology, Yokohama, Japan

7
8 Corresponding author: Yoko Yamagami (y.yamagami@jamstec.go.jp)

9 † Research Center for Environmental Modeling and Application, Japan Agency for Marine-Earth
10 Science and Technology, 3173-25 Showamachi, Kanazawaku, Yokohama, Kanagawa 236-0001,
11 Japan

12
13 **Key Points:**

- 14 • Reproducibility of sea level variability is compared along the western coast of India using
15 eddy-resolving and non-eddy ocean models.
- 16 • The eddy-resolving model captures coastal Kelvin waves arising from Indian Ocean
17 dipole and consequent intraseasonal sea level variations.
- 18 • The non-eddy model may miss over 81% of the extreme sea level events compared to
19 observations.
- 20
21

22 Abstract

23 Future sea level rise under global warming poses serious risks of extreme sea level events in
24 coastal regions worldwide. Numerous state-of-the-art climate models, with their relatively coarse
25 horizontal resolution, may not adequately resolve coastal wave dynamics, leading to
26 uncertainties in coastal sea level variability representation. This study compared eddy-resolving
27 and non-eddy ocean models in reproducing sea level variability, focusing on the probability
28 distribution along the western coast of India. The eddy-resolving model can simulate
29 intraseasonal sea level variations associated with coastal waves driven by equatorial wind
30 anomalies. The non-eddy model fails to capture over 81% of observed extreme sea level
31 events, as shown in the probability distribution for intraseasonal time series. Although capable of
32 simulating Indian Ocean Dipole-related low-frequency sea level anomalies, the non-eddy
33 model does not replicate their connection to intraseasonal extreme events. The results suggest
34 that climate model projections may underestimate future changes in extreme sea level events.

35

36 Plain Language Summary

37 Sea level variations in the northern Indian Ocean are influenced by ocean waves near the coast,
38 typically in a horizontal scale of approximately 100 km. It is not clear if these coastal waves and
39 their movement are accurately represented in climate simulations, which typically have a relatively
40 coarse horizontal resolution. This study compared sea level variations along the western coast of
41 India using two ocean models with coarse and fine horizontal resolutions. We found that the
42 high-resolution model adequately simulates the generation and propagation of coastal waves, and
43 thus successfully simulates sea level variations with a 20–150-day time scale along western India.
44 This result suggests that many recent climate simulations may have underestimated the
45 frequency of extreme sea level events in coastal regions.

46

47 1 Introduction

48 Global warming is projected to cause persistent sea level rise worldwide (IPCC 2022a). In
49 addition to the global mean sea level rise owing to thermal expansion, melting of glaciers, etc.,
50 extreme sea level projections associated with changes in atmospheric circulation and river runoff
51 are also required in coastal regions, especially projections of changes in the occurrence of

52 extreme events (IPCC 2022b). Given that many of the state-of-art climate models in the Coupled
53 Model Intercomparison Project Phase 6 (CMIP6) use a relatively coarse horizontal resolution of
54 approximately 100 km, the projections obtained using these models may underestimate influence
55 of oceanic mesoscale structures and coastal phenomena. Hence, it remains unclear whether
56 current sea level projections, particularly in coastal regions, adequately capture changes in
57 extreme sea level events (i.e., as indicated by the tails in probability distributions).

58 In the densely populated coastal areas of the northern Indian Ocean, projected sea level rises in
59 the Arabian Sea and the Bay of Bengal (Han et al., 2010; Jyoti et al., 2023) present serious risks,
60 including coastal storm surges and extreme tidal events. Sea level variability along the coasts of
61 the northern Indian Ocean is strongly influenced by equatorial waves and their resultant coastal
62 Kelvin wave. Clarke and Liu (1994) showed that the interannual sea level anomalies (SLA)
63 along the coasts of the northern Indian Ocean were remotely triggered by equatorial zonal winds.
64 More recently, using linear stratified models (McCreary, 1996), several studies have investigated
65 how wind stress forcing over the Arabian Sea, the southern tip of Sri Lanka, and the equatorial
66 Indian Ocean impacts intraseasonal-to-interannual sea level variations along the coast of India
67 (Suresh et al., 2013, 2016, 2018). Wind variations leading to coastal Kelvin waves can be
68 attributed to semiannual basin-scale wind variability that drives the equatorial jet (Yoshida,
69 1959; Wyrтки, 1973), intraseasonal anomalies associated with the Madden-Julian Oscillation
70 (MJO; Madden & Julian, 1977), and interannual anomalies associated with the Indian Ocean
71 Dipole (IOD) (Saji et al., 1999; Han & Webster, 2002; Aparna et al., 2012).

72 Although previous studies suggested the potential role of coastal Kelvin waves in the Northern
73 Indian Ocean, the extent to which standard climate models reproduce the coastal sea level
74 variations remains unclear. Therefore, using the coastal sea level variability along western India
75 as an illustrative example, this study undertakes a comparative analysis of multiple simulations
76 derived from the oceanic component utilized in a climate model. Here we show that an eddy-
77 resolving ocean general circulation model (OGCM) is required to accurately represent sea level
78 variations along the western coast of India. In particular, since intraseasonal sea level variations
79 have a relatively pronounced amplitude and consequently lead to extreme events, this study
80 focuses mainly on how the intraseasonal variations in coastal sea level are represented in
81 OGCMs. Even though the non-eddy OGCM simulation is forced by the same atmospheric
82 boundary conditions as in the eddy-resolving OGCM, the coarse horizontal resolution of the non-

83 eddying OGCM fails to accurately capture the sea level variability, especially variations
84 originating from the equator through the coastal wave guide in the Bay of Bengal.

85 **2 Models, Data, and Methods**

86 This study compares two simulations of CCSR Ocean Component Model (COCO) (Hasumi,
87 2006), which serves as the sea ice-ocean component of the sixth version of the Model for
88 Interdisciplinary Research on Climate (MIROC6; Tatebe et al., 2019) that was developed
89 cooperatively by the Japanese climate modeling community. The configurations of the coarse
90 stand-alone OGCM used in the present study are exactly the same as the global OGCM
91 component of MIROC6. The model employs a nominal 1° horizontal resolution in a tripolar
92 coordinate system, and there are 63 vertical levels, including the lowermost layer that
93 incorporates bottom boundary layer parameterization (Nakano & Suginoara, 2002). This
94 simulation is referred to as “COCO-LR” hereafter. We also used a global high-resolution version
95 of COCO, which has horizontal resolution of 0.1° (hereafter referred to as COCO-HR). Using
96 the phase 2 protocol of the Ocean Model Intercomparison Project (OMIP2; Tsujino et al., 2020),
97 an endorsed Multi-Model Intercomparison Project (MIP) of CMIP6, both models were initialized
98 using observed temperature and salinity data from the World Ocean Atlas 2013 version 2
99 (Locarnini et al., 2013; Zweng et al., 2013). The models were driven by JRA55-do 3-hourly
100 surface forcings (Tsujino et al., 2020) from 1958 to 2019 for COCO-HR and to 2018 for COCO-
101 LR (Komuro, 2019). In the COCO-HR model, regardless of the existence of sea ice, sea surface
102 salinity (SSS) above the latitudes of 60°N and below 60°S was weakly relaxed to observational
103 data with a 10-day restoring timescale to avoid model drift. Similarly, temperature and salinity at
104 depths greater than 1500 m were also restored to observed values with a 5-year timescale. Note
105 that COCO-HR improved the representation of the mean state in the Indian Ocean (see Text S1
106 for details).

107 To highlight the impact of interannual variations in surface wind forcing on the coastal sea
108 level along the western coast of India, we also conducted a sensitivity experiment, hereafter
109 referred to as “WIND0”. In this experiment, we used only the 3-hourly climatological mean of
110 surface wind data for calculating surface wind stresses in COCO-HR. Thus, the surface wind
111 stresses (i.e., dynamical forcing) in WIND0 incorporate only climatological mean variations,
112 excluding low-frequency variations that occur over periods longer than 1 year. Other surface

113 forcings in WIND0, such as surface heat flux, freshwater flux, and river runoff (i.e.,
114 thermodynamical forcing), are the same as those in COCO-HR.

115 In this study, we used the following observational datasets. PCMDI-SST (Hurrell et al., 2008)
116 was used for the monthly sea surface temperature (SST) data for the period 1993–2019 with a
117 horizontal resolution $1^\circ \times 1^\circ$, as in Tsujino et al. (2020). CMEMS sea level products (DUACS
118 DT2014; Pujol et al., 2016) have a daily interval and a horizontal resolution of $0.25^\circ \times 0.25^\circ$ for
119 the period 1993–2019. Drifter-derived monthly climatological surface currents data were also
120 used (Laurindo et al., 2017). To compare sea level anomalies with the satellite altimeter
121 products, we mainly analyzed model outputs after 1993.

122 To examine SLA propagation in the coastal area, we calculated lag composites of SLA for
123 extreme sea level events. A two-tailed *t*-test was adapted to the statistical test at 90% confidence
124 level. To estimate the probability density functions (PDFs) of SLA, Kernel Density estimation
125 was applied (Dehand, 1987; Marshall & Molteni, 1993). A Butterworth filter was employed to
126 isolate the intraseasonal variability within the 20-150 day period.

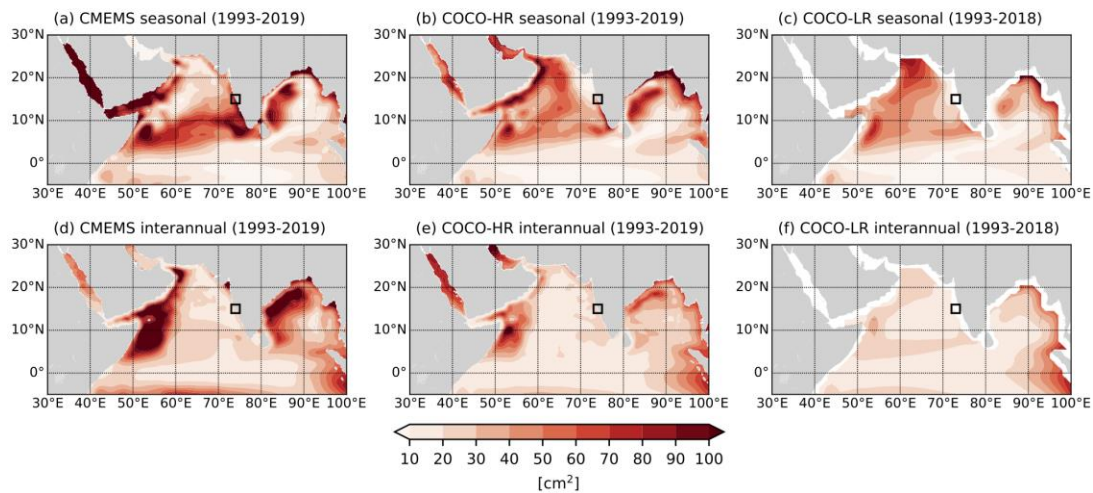
127

128 **3 Sea level variance in the Northern Indian Ocean**

129 In this section, we briefly validate the COCO-HR model focusing on sea level variability.
130 COCO-HR showed noticeable improvements in the northern Indian Ocean, especially in regions
131 where oceanic mesoscale eddies are dominant (Fig. 1). Regarding seasonal variability,
132 observational data showed large-amplitude sea level variance in the Arabian Sea and the Bay of
133 Bengal (Fig. 1a). These patterns are explained by the seasonal dynamics of the Lakshadweep
134 High/Low in the southern Arabian Sea (Vinayachandran et al., 2007) and coastal wave guide
135 effect in the Bay of Bengal (Clarke & Liu, 1994). The general structure of this seasonal sea level
136 variability is well represented in the COCO-HR model, both in terms of spatial pattern and
137 amplitude (Fig. 1b). Although the COCO-LR model showed a similar pattern, the overall
138 amplitude was smaller than that in COCO-HR (Fig. 1c), suggesting that the coarse resolution
139 model underestimates the seasonal sea level variability in the northern Indian Ocean.

140 In addition, COCO-HR more accurately captures detrended interannual SLAs compared to
141 COCO-LR (Fig. 1d-f). The noticeable interannual variations in the Somalia-Oman upwelling
142 region are well represented in COCO-HR, aligning closely with observations, although COCO-

143 HR does slightly underestimate them. This difference is presumably because the interannual
 144 variability of the mesoscale variability associated with the Somali Current is well represented in
 145 COCO-HR. Interannual sea level variability in the western Bay of Bengal also tends to be better
 146 represented in COCO-HR, indicating that the interannual variability of coastal trapped waves
 147 and local mesoscale variability is also well captured by COCO-HR. In the following section, we
 148 examined sea level variations along the western coast of India in greater detail.
 149



150
 151 **Figure 1.** Variances in seasonal sea level anomalies (SLAs) [cm^2] in the northern Indian Ocean
 152 for (a) observations, (b) COCO-HR, and (c) COCO-LR. (d)-(f) As in (a)-(c), but for interannual
 153 SLAs. Interannual anomalies are defined as detrended anomalies from the climatology.

154 4 SLAs along the western coast of India

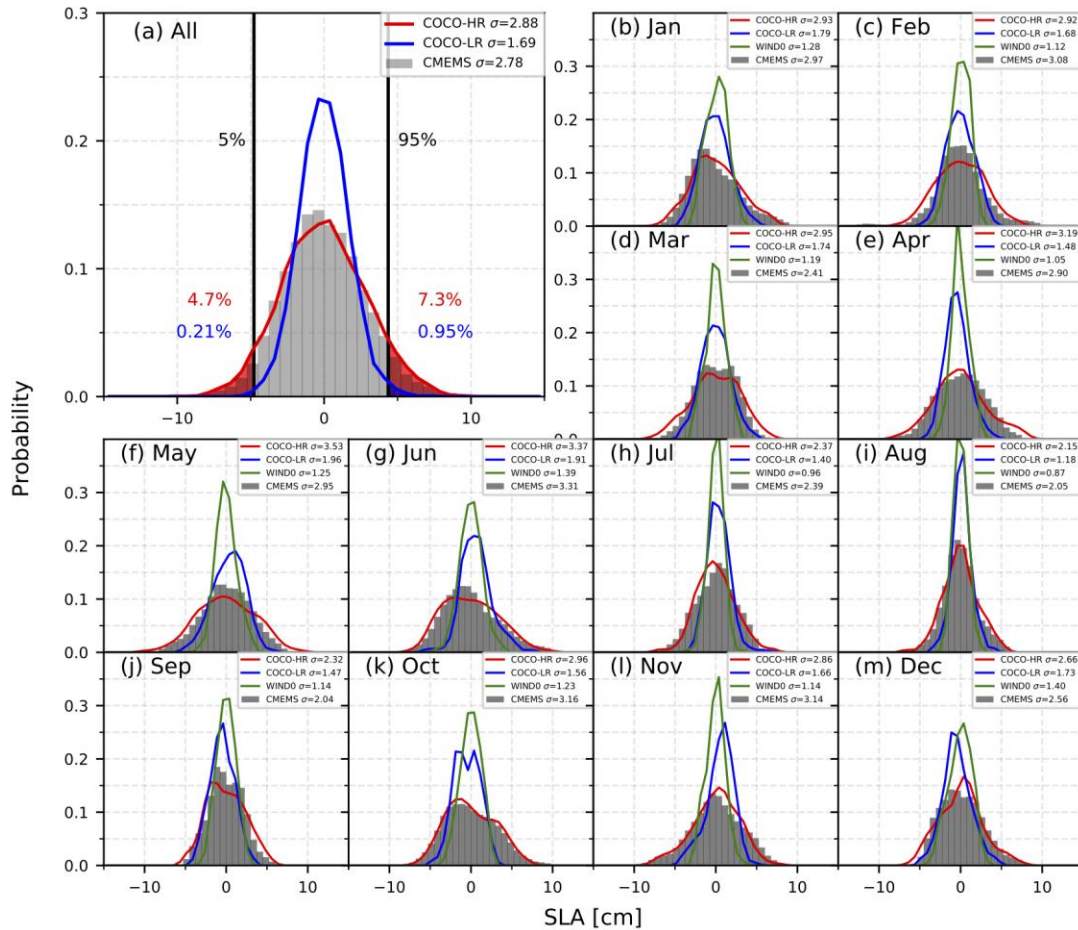
155 4.1 Intraseasonal sea level variations

156 In order to investigate sea level variations along the western coast of India, area-averaged sea
 157 level variations are calculated within $2^\circ \times 2^\circ$ boxes at 15°N (black boxes in Fig. 1). Note that
 158 qualitatively similar results are obtained if we use $1^\circ \times 1^\circ$ boxes. The comparison indicates that
 159 COCO-HR more accurately represents both seasonal (Text S2) and intraseasonal SSH variations
 160 along the west coast of India.

161 PDFs for 20-150 day band-passed SLA time series are estimated (Fig. 2). Note that we refer to
 162 the 20-150 day band-passed timeseries of detrended anomalies from the daily climatology as
 163 “intraseasonal anomalies” hereafter. In all months, COCO-HR reproduces PDFs that are similar

164 to the observational data, with standard deviations that also match those of the observational
165 data. Conversely, COCO-LR exhibits smaller standard deviations for each PDF compared to the
166 observations, resulting in underestimation of extreme SLA events. Indeed, in the observational
167 data, the thresholds employed for positive (negative) extreme SLA events, i.e., events exceeding
168 95% (5.0%) probability, are estimated to be 4.4 cm (-4.8 cm) (Fig. 2a). For COCO-HR, the
169 occurrence rates of positive (negative) extreme SLA events are 7.3% (4.7%), which is consistent
170 with the observed rates. For COCO-LR, the occurrence of positive (negative) SLA events is
171 0.95% (0.21%), which is considerably smaller than in the observations. This result means that
172 COCO-LR misses 81% (96%) of the extreme intraseasonal sea level maxima (minima), and
173 underscores the importance of using an eddy-resolving ocean model to accurately hindcast
174 coastal sea level variability.

175 The narrower PDFs (i.e., indicating less variance) in WIND0 compared to COCO-HR
176 suggests a reduced occurrence of extreme SLA events. Therefore, dynamical wind forcing
177 anomalies are necessary for simulating intraseasonal SLA along the western coast of India (Fig.
178 2b-m). This result also implies that the contribution of factors other than wind stress forcing,
179 such as buoyancy flux and baroclinic instability associated with West Indian Coastal Current
180 (e.g., Varna et al., 2023), is not predominant. The above result remains qualitatively unchanged
181 if the PDFs are calculated for detrended anomalies without 20–150-day bandpass filtering (Fig.
182 S5). Thus, differences in anomalies with periods shorter (longer) than 20 (150) days do not
183 explain the reduction in the standard deviation of PDFs in WIND0. Consequently, the higher
184 frequency of extreme SLA events in COCO-HR can be attributed to interannual-to-decadal
185 changes in the intraseasonal anomalies. Given that the variance in the intraseasonal component
186 is prominent in both the observation and models (Fig. S6), compared to the total variance, we
187 will discuss the processes driving these differences in PDFs of intraseasonal variability in the
188 next section.



189

190 **Figure 2.** Probability density functions (PDFs) of intraseasonal (20-150 days) sea level
 191 anomalies (SLA) [cm] along the western coast of India (15°N) for observations (CMEMS; black
 192 bars), COCO-HR (red lines), COCO LR (blue lines), and WIND0 (green lines) for (a) all seasons
 193 and (b)-(m) each month. PDFs are estimated by kernel density estimation. The standard
 194 deviation (σ) for each month is given in the legend accompanying each graph. All PDFs are
 195 normalized and the vertical axis indicates probability (unit less). In (a), vertical black lines
 196 indicate the 5% and 95% anomalies based on CMEMS data. Areas where anomalies exceed the 5
 197 or 95 percentiles for CMEMS are highlighted in red (COCO-HR) and blue (COCO-LR) colors,
 198 respectively, with the corresponding percentile values marked in each model.

199

200 4.2 Resolution dependency of the propagation of coastal Kelvin waves

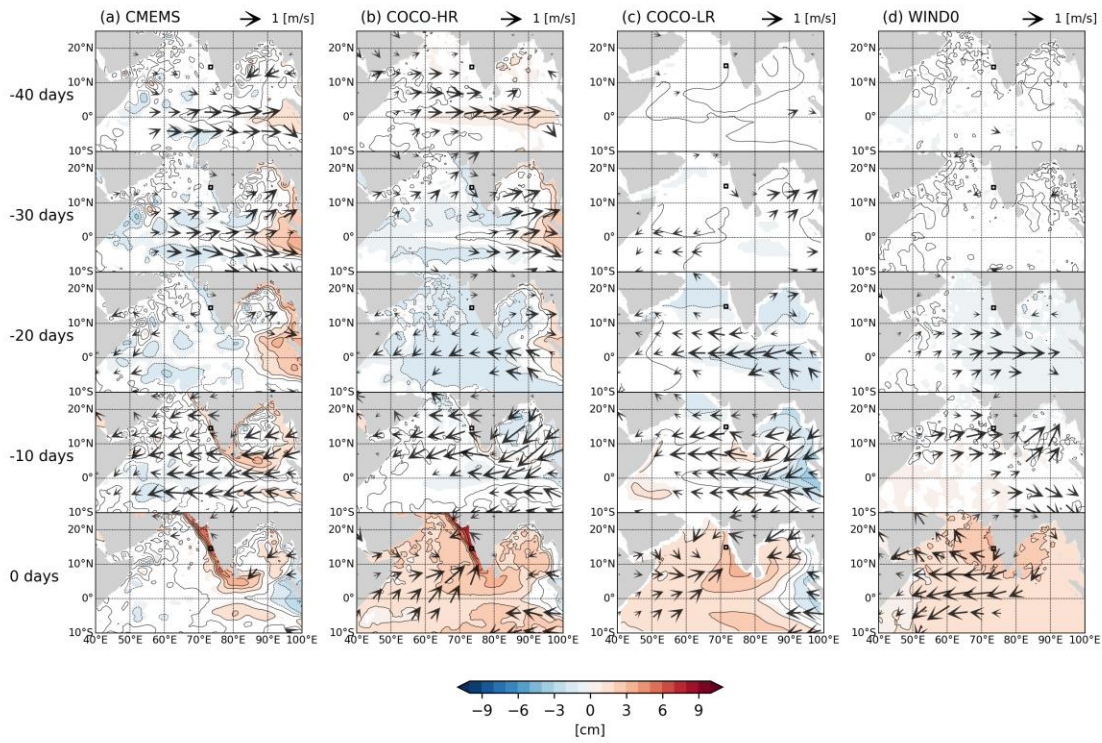
201 Regarding the remote impacts of coastal Kelvin waves on the western coast of India, the large

202 intraseasonal SLA variances in COCO-HR may be attributed to the propagation of sea level
203 anomalies. Figure 3 shows a lag composite of SLA from 0 to 40 days before the occurrence of
204 intraseasonal SLA exceeds +1 standard deviation at the western coast of India (indicated by red
205 symbols in Fig. S6). Since the composites obtained for the negative anomalies are almost mirror
206 images, we discuss only the results obtained for positive SLA events. In the observations, a
207 significant SLA associated with equatorial Kelvin wave is triggered by westerly wind anomalies
208 in the tropical Indian Ocean 40 days prior. Subsequently, this wave reaches the coast of Sumatra
209 island and then propagates as coastal Kelvin waves along the coast of the Bay of Bengal. These
210 waves pass through the southern tip of India, arrive at the western coast of India, and eventually
211 extend into the northern Arabian Sea (Fig. 3a). Furthermore, SLAs also appear to be radiated
212 from the eastern coast of the Bay of Bengal as westward Rossby waves, and are enhanced by
213 easterly wind anomalies along the southern tip of Sri Lanka.

214 In COCO-HR, similar to the observations, the equatorial Kelvin wave enters the eastern
215 boundary and propagates as coastal Kelvin waves from the Bay of Bengal to the western coast of
216 India (Fig. 3b). Westward SLAs also appeared to be radiated from the eastern coast of the Bay of
217 Bengal to the southern coast of India. On the other hand, COCO-LR does not show SLA
218 propagation in the coastal region from the equator to the Bay of Bengal. Instead, positive SLAs
219 appear to develop locally about 10 days prior, before rapidly increasing in the western coast of
220 India. Previous studies proposed that intraseasonal SLA variations along the western coast of
221 India are predominantly influenced by the propagation of the coastal Kelvin waves from the
222 equatorial Indian Ocean (Suresh et al., 2013). Therefore, the results obtained in this study
223 suggest that COCO-HR effectively captures the propagation of coastal Kelvin waves from the
224 equator. However, the propagation of Kelvin waves from the equator is not well captured by
225 COCO-LR due to the coarser horizontal resolution (Text S3), suggesting an exaggerated
226 influence of local wind and/or thermal forcing in the western coast of India.

227 In the WIND0 composites, no SLA propagation originating from the equatorial Kelvin waves
228 is evident. This is because the suppressed wind stress anomalies do not trigger intraseasonal
229 anomalies of the equatorial Kelvin waves and, consequently, the coastal Kelvin waves in the Bay
230 of Bengal. These results are also supported by the lag-composite analysis of SLA from 0 to 40
231 days following instances when the SLA exceeds +1 standard deviation at the eastern equatorial
232 Indian Ocean (Fig. S7). While both COCO-HR and COCO-LR depict the propagation of

233 equatorial Kelvin waves to the eastern boundary, only the observations and COCO-HR show the
 234 subsequent SLA propagation in the Bay of Bengal.



235

236 **Figure 3.** Lag-composites of sea level anomalies (SLA) (contour and color) and 10-m wind
 237 (vectors) for area-averaged SLA time series along the western coast of India (black boxes). Data
 238 are shown for (a) CMEMS, (b) COCO-HR, (c) COCO-LR, and (d) WIND0. Colors and vectors
 239 indicate statistically significant SLA and zonal wind anomalies at the 90% confidence level,
 240 respectively.

241

242 **4.3 Influence of Indian Ocean Dipole on the probability distribution of coastal SLA along** 243 **the western coast of India**

244 In section 4.2, differences in PDFs of intraseasonal SLA are attributed to the representation of
 245 coastal Kelvin waves. This section examines the origin of the coastal Kelvin waves, particularly
 246 their association with wind variations in the tropical Indian Ocean. Given that basin-scale wind
 247 anomalies in the tropical Indian Ocean are affected by the IOD, it follows that the IOD
 248 contributes to interannual low-frequency SLA variations along the western coast of India through
 249 coastal Kelvin waves (e.g., Suresh et al., 2018). However, the extent to which interannual wind

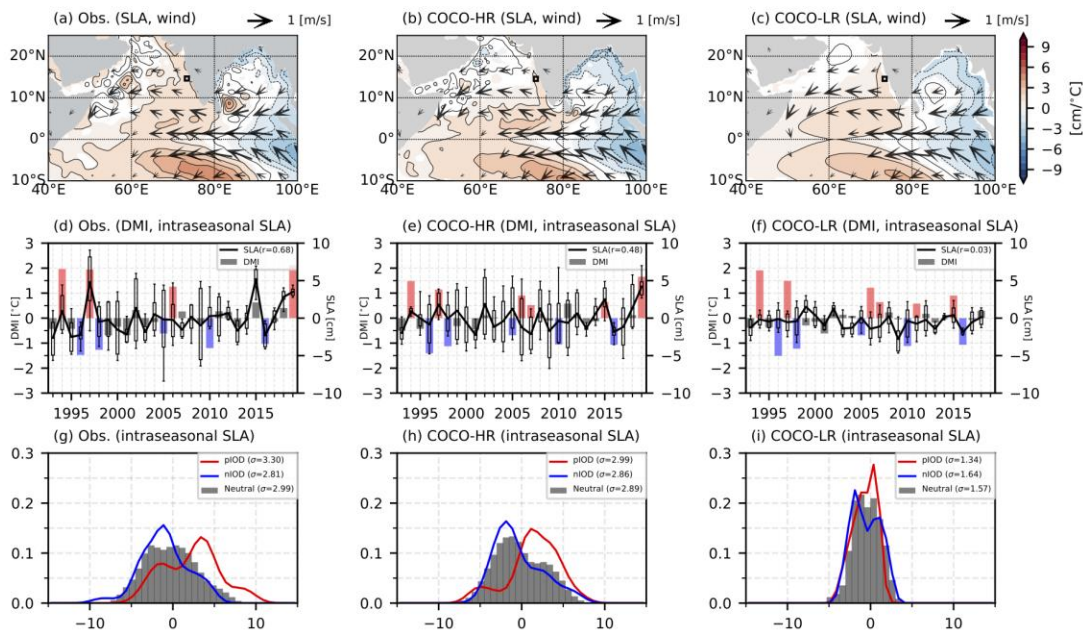
250 anomalies associated with the IOD modulate intraseasonal SLA variations, specifically the
251 probability distribution of coastal SLA along the western coast of India, remains unclear. We
252 therefore investigated the relationship between IOD and intraseasonal SLA, and assessed its
253 representation in both COCO-HR and COCO-LR. In this analysis, the dipole mode index (DMI)
254 is defined as the difference between area-averaged monthly-mean SST difference between the
255 western (50°E-70°E, 10°S-10°N) and eastern (90°E-110°E, 10°S-0°) poles, as defined in
256 previous studies (Saji et al., 1999; Tanizaki et al., 2017). A 3-month running mean is also applied
257 to the DMI.

258 Since SST anomalies associated with the IOD typically peak in October (e.g., Saji et al.,
259 1999), we focus on the relationship between the IOD and intraseasonal SLA along the western
260 coast of India during this month. During positive IOD events, equatorial easterly wind anomalies
261 trigger positive (negative) SLAs along the southern tip of Sri Lanka (in the eastern equatorial
262 Indian Ocean) and, subsequently, positive (negative) coastal Kelvin waves along the western
263 coast of India (coastal region of the Bay of Bengal) as observed (Fig. 4a). The SLAs associated
264 with the IOD affects the interannual modulation of intraseasonal SLAs along the western coast of
265 India (Fig. 4d). The correlation between the October-mean of intraseasonal SLAs and the DMI is
266 0.68, indicating that the IOD modulates the interannual variations in intraseasonal SLA. During
267 the positive IOD phases, the PDF of the intraseasonal SLA shifts positively (Fig. 4g).
268 Conversely, the PDFs during negative IOD and neutral years are less distinct, which may be
269 attributed to the asymmetry in the IOD, with negative events having a smaller amplitude than
270 positive events (e.g., Nakazato et al., 2021, An et al., 2023).

271 COCO-HR can simulate positive SLAs along the west Indian coast during the positive IOD
272 (Fig. 4b). Also, the relatively strong correlation between intraseasonal SLA and DMI ($r=0.48$)
273 are moderately represented (Fig. 4e), and the PDF shifts positively during positive IOD phases,
274 as observed (Fig. 4h). On the other hand, although the SLA patterns along the west coast of India
275 are similar during the IOD (Fig. 4a-c), intraseasonal SLAs are not correlated with the DMI
276 ($r=0.03$) and the PDF does not shift positively in COCO-LR (Fig. 4f, i).

277 While both COCO-HR and COCO-LR are driven by the same surface forcings, leading to
278 similar large-scale SLA variation patterns in October, there are notable differences at a local
279 scale. This discrepancy is particularly evident when focusing on the local SLA along the western
280 coast of India, where COCO-LR fails to represent the interannual variations. Additionally,

281 COCO-LR underestimates the variability in SLAs associated with intraseasonal variations, and
 282 the differences in PDFs between the IOD phases are not adequately represented (Fig. 4; Fig. S9).
 283 This issue in COCO-LR is likely due to its inability to adequately represent the propagation
 284 process of coastal waves originating from the equator, as discussed in the previous section.
 285 Therefore, we conclude that interannual wind anomalies associated with the IOD influence the
 286 occurrence of extreme SLAs along the western coast of India, and that this effect is represented
 287 in the eddy-resolving ocean model. Furthermore, while the non-eddy model can represent the
 288 low-frequency SLA patterns associated with the IOD, it lacks the necessary resolution to
 289 simulate modulations in extreme intraseasonal SLAs.



290
 291 **Figure 4.** (a) Regressions of October-mean sea level anomalies (SLAs) and 10 m wind
 292 anomalies to September-October-November (SON)-mean dipole mode index (DMI) for CMEMS
 293 and JRA55-do data. Colors and vectors indicate statistically significant regression coefficients
 294 for SLAs and zonal winds at the 90% confidence level, respectively. (d) Time series of the DMI
 295 (bar) and intraseasonal SLA (i.e., bandpassed for 20-150 days) (line) during October along the
 296 western Indian coast (15°N; black box in (a)), based on observational data. The correlation
 297 between DMI and October-mean intraseasonal SLA is shown in the legend of each graph. Red
 298 (blue) bars indicate positive (negative) IOD, while gray bars indicate neutral years. Daily
 299 intraseasonal SLAs for a 31-day period, October, are depicted using box-whisker plots, where
 300 boxes span the 25% to 75% ranges in the data, the line indicates the monthly mean, and the

301 whiskers indicate the 5% to 95% ranges in the data. (g) PDFs for intraseasonal SLAs based on
302 observational data for October, as in Fig. 2, but for during positive IOD years (red line), negative
303 IOD years (blue line), and neutral years (gray bars). (b),(e),(h) As in (a), (d), (g), but for COCO-
304 HR. (c),(f),(i) As in (a),(d),(g), but for COCO-LR.

305

306 **5 Summary and discussion**

307 This study showed that only the eddy-resolving OGCM (COCO-HR) is capable of
308 reproducing the intraseasonal variability of SLAs along the western coast of India. The results
309 indicate that COCO-HR effectively represents extreme SLA events along the western coast of
310 India. Conversely, the non-eddy model (COCO-LR) fails to capture more than 81% of these
311 extreme intraseasonal sea level events. In the COCO-HR model, equatorial Kelvin waves
312 originating in the equatorial ocean enter the eastern boundary and subsequently propagate along
313 the coast of the Bay of Bengal and western India, while COCO-LR fails it due to the coarser
314 horizontal resolution. Furthermore, changes in the PDFs of intraseasonal SLAs associated with
315 the IOD are captured only in the COCO-HR model. This suggests that basin-scale wind
316 anomalies in the equatorial Indian Ocean can modulate the occurrence of extreme SLA events
317 along the western coast of India.

318 The underestimation of coastal extreme sea level events in the non-eddy OGCM further
319 implies that such extremes may be underestimated in CMIP6 models. In the context of recent
320 research on extreme weather events and their links to a warming climate, several studies have
321 emphasized the large-scale drivers of local extreme events (Kawase et al., 2019; Imada et al.,
322 2020). Our results show that the probability of local sea level extremes along the western coast
323 of India is also affected by large-scale wind anomalies associated with the IOD, thus
324 demonstrating a "global-to-local" approach in oceanic contexts. While this study focused on the
325 IOD, future studies should examine the impacts of intraseasonal atmospheric variability, such as
326 the MJO and the Boreal Summer Intraseasonal Oscillation (Wang & Xie, 1997) on coastal SLAs.
327 Consequently, a reassessment of the risk of extreme sea level events, such as storm surges and
328 floods in the coastal areas of the North Indian Ocean, may be needed. This reassessment should
329 focus on the resolution of ocean models to better understand the relationship between changes in
330 local coastal sea level extremes and basin-scale climate variability under global warming.

331

332 **Acknowledgments**

333 This work was supported by the MEXT program for advanced studies of climate change
334 projection (SENTAN) (Grant Number JPMXD0722680395), and also by a joint research
335 program between the Ministry of Earth Sciences (MoES) in India and JAMSTEC on ocean
336 downscaling of climate model projections in Indian coastal regions to assess the coastal impact
337 of sea level rise under conditions of global warming. The first author was supported by JSPS
338 KAKENHI Grant Numbers JP20H05729, JP22K14098, and JP22H04487.

339

340 **Open Research**

341 The altimeter products were produced and distributed by Copernicus Marine Environment
342 Monitoring Service (<https://doi.org/10.48670/moi-00148>). Drifter-derived data was downloaded
343 from https://www.aoml.noaa.gov/ftp/phod/pub/lumpkin/drifter_climatology/. JRA55-do data
344 (<https://esgf-node.llnl.gov/search/input4mips>), PCMDI-SST
345 (https://aims2.llnl.gov/search/input4mips/?institution_id=PCMDI&source_version=1.1.9), and
346 COCO-LR outputs ([http://esgf-](http://esgf-node.llnl.gov/search/cmip6/?mip_era=CMIP6&activity_id=OMIP&institution_id=MIROC&source_id=MIROC6&experiment_id=omip2)
347 [node.llnl.gov/search/cmip6/?mip_era=CMIP6&activity_id=OMIP&institution_id=MIROC&source_id=MIROC6&experiment_id=omip2](http://esgf-node.llnl.gov/search/cmip6/?mip_era=CMIP6&activity_id=OMIP&institution_id=MIROC&source_id=MIROC6&experiment_id=omip2)) are now distributed through the Earth System Grid
348 Federation. The COCO-HR and WIND0 data have been deposited in the Zenodo
349 (<https://doi.org/10.5281/zenodo.10633562>).

351

352 **References**

- 353 1. An, S. I., Park, H. J., Kim, S. K., Cai, W., Santoso, A., Kim, D., & Kug, J. S. (2023). Main
354 drivers of Indian Ocean Dipole asymmetry revealed by a simple IOD model. *npj Climate*
355 *and Atmospheric Science*, 6(1), 93. <https://doi.org/10.1038/s41612-023-00422-2>
- 356 2. Aparna, S. G., McCreary, J. P., Shankar, D., & Vinayachandran, P. N. (2012). Signatures of
357 Indian Ocean Dipole and El Niño–Southern Oscillation events in sea level variations in the
358 Bay of Bengal. *Journal of Geophysical Research*, 117, C10012.
359 <https://doi.org/10.1029/2012JC008055>
- 360 3. Chelton, D. B., deSzoeko, R. A., Schlax, M. G., Naggar, K. E., & Siwertz, N. (1998).

- 361 Geographical variability of the first baroclinic Rossby radius of deformation. *Journal of*
 362 *Physical Oceanography*, 28, 433–460, [https://doi.org/10.1175/1520-](https://doi.org/10.1175/1520-0485(1998)028,0433:GVOTFB.2.0.CO;2)
 363 0485(1998)028,0433:GVOTFB.2.0.CO;2.
- 364 4. Clarke, A. J., & Liu, X. (1994). Interannual sea level in the northern and eastern Indian
 365 Ocean. *Journal of Physical Oceanography*, 24(6), 1224-1235.
- 366 5. Dehnad, K. (1987). Density estimation for statistics and data analysis.
 367 *Technometrics*, 29:4, 495, <https://doi.org/10.1080/00401706.1987.10488295>
- 368 6. Gill, A. E. (1982). *Atmosphere-ocean dynamics*. New York: Academic Press.
- 369 7. Gordon, A. L., Sprintall, J., Van Aken, H. M., Susanto, D., Wijffels, S., Molcard, R., et al.
 370 (2010). The Indonesian throughflow during 2004–2006 as observed by the INSTANT
 371 program. *Dynamics of Atmospheres and Oceans*, 50(2), 115-128.
 372 <https://doi.org/10.1016/j.dynatmoce.2009.12.002>.
- 373 8. Han, W., & Webster, P. J. (2002). Forcing mechanisms of sea level interannual variability in
 374 the Bay of Bengal. *Journal of Physical Oceanography*, 32(1), 216-239.
 375 [https://doi.org/10.1175/1520-0485\(2002\)032<0216:FMOSLI>2.0.CO;2](https://doi.org/10.1175/1520-0485(2002)032<0216:FMOSLI>2.0.CO;2)
- 376 9. Han, W., Meehl, G. A., Rajagopalan, B., Fasullo, J. T., Hu, A., Lin, J., et al. (2010). Patterns
 377 of Indian Ocean sea-level change in a warming climate. *Nature Geoscience*, 3(8), 546-550.
 378 <https://doi.org/10.1038/ngeo901>
- 379 10. Han, W., McCreary, J. P., Masumoto, Y., Vialard, J., & Duncan, B. (2011). Basin
 380 resonances in the equatorial Indian Ocean. *Journal of Physical Oceanography*, 41(6), 1252-
 381 1270. <https://doi.org/10.1175/2011JPO4591.1>
- 382 11. Hasumi, H., 2006: CCSR Ocean Component Model (COCO) version 4.0. *CCSR Technical*
 383 *Report*, 25, 103 pp., <https://ccsr.aori.utokyo.ac.jp/hasumi/COCO/coco4.pdf>.
- 384 12. Hurrell, J. W., Hack, J. J., Shea, D., Caron, J. M., & Rosinski, J. (2008). A new sea surface
 385 temperature and sea ice boundary dataset for the Community Atmosphere Model. *Journal of*
 386 *Climate*, 21(19), 5145-5153. <https://doi.org/10.1175/2008JCLI2292.1>
- 387 13. Imada, Y., Kawase, H., Watanabe, M., Arai, M., Shiogama, H., & Takayabu, I. (2020).
 388 Advanced risk-based event attribution for heavy regional rainfall events. *npj climate and*
 389 *atmospheric science*, 3(1), 37. <https://doi.org/10.1038/s41612-020-00141-y>
- 390 14. Intergovernmental Panel on Climate Change (IPCC). (2022a). Sea Level Rise and
 391 Implications for Low-Lying Islands, Coasts and Communities. In *The Ocean and*

- 392 *Cryosphere in a Changing Climate: Special Report of the Intergovernmental Panel on*
393 *Climate Change* (pp. 321–446). chapter, Cambridge: Cambridge University Press.
394 <https://doi.org/10.1017/9781009157964.006>
- 395 15. Intergovernmental Panel on Climate Change (IPCC). (2022b). Extremes, Abrupt Changes
396 and Managing Risks. In *The Ocean and Cryosphere in a Changing Climate: Special Report*
397 *of the Intergovernmental Panel on Climate Change* (pp. 589–656). Cambridge: Cambridge
398 University Press. <https://doi.org/10.1017/9781009157964.008>.
- 399 16. Jyoti, J., Swapna, P., & Krishnan, R. (2023). North Indian Ocean sea level rise in the past
400 and future: The role of climate change and variability. *Global and Planetary Change*, 228,
401 104205. <https://doi.org/10.1016/j.gloplacha.2023.104205>
- 402 17. Kawase, H., Imada, Y., Sasaki, H., Nakaegawa, T., Murata, A., Nosaka, M., & Takayabu, I.
403 (2019). Contribution of historical global warming to local-scale heavy precipitation in
404 western Japan estimated by large ensemble high-resolution simulations. *Journal of*
405 *Geophysical Research: Atmospheres*, 124(12), 6093-6103.
406 <https://doi.org/10.1029/2018JD030155>
- 407 18. Komuro, Y. (2019). *MIROC MIROC6 model output prepared for CMIP6 OMIP*
408 *omip2*. Version YYYYMMDD. Earth System Grid
409 Federation. <https://doi.org/10.22033/ESGF/CMIP6.5655>
- 410 19. Laurindo, L. C., Mariano, A. J., & Lumpkin, R. (2017). An improved near-surface velocity
411 climatology for the global ocean from drifter observations. *Deep Sea Research Part I:*
412 *Oceanographic Research Papers*, 124, 73-92. <https://doi.org/10.1016/j.dsr.2017.04.009>
- 413 20. Locarnini, M. M., Mishonov, A. V., Baranova, O. K., Boyer, T. P., Zweng, M. M., Garcia,
414 H. E., et al. (2018). World ocean atlas 2018, volume 1: Temperature. NOAA Atlas NESDIS
415 81, 52pp. <https://archimer.ifremer.fr/doc/00651/76338/>
- 416 21. Madden, R. A., & Julian, P. R. (1971). Detection of a 40–50 day oscillation in the zonal
417 wind in the tropical Pacific. *Journal of Atmospheric Sciences*, 28(5), 702-708.
418 [https://doi.org/10.1175/1520-0469\(1971\)028%3C0702:DOADOI%3E2.0.CO;2](https://doi.org/10.1175/1520-0469(1971)028%3C0702:DOADOI%3E2.0.CO;2)
- 419 22. Marshall, J., & Molteni, F. (1993). Toward a dynamical understanding of planetary-scale
420 flow regimes. *Journal of the Atmospheric Sciences*, 50(12), 1792-1818.
421 [https://doi.org/10.1175/1520-0469\(1993\)050%3C1792:TADUOP%3E2.0.CO;2](https://doi.org/10.1175/1520-0469(1993)050%3C1792:TADUOP%3E2.0.CO;2)

- 422 23. McCreary Jr, J. P., Kundu, P. K., & Molinari, R. L. (1993). A numerical investigation of
423 dynamics, thermodynamics and mixed-layer processes in the Indian Ocean. *Progress in*
424 *Oceanography*, 31(3), 181-244. [https://doi.org/10.1016/0079-6611\(93\)90002-U](https://doi.org/10.1016/0079-6611(93)90002-U)
- 425 24. Nakano, H., & Suginoara, N. (2002). Effects of bottom boundary layer parameterization on
426 reproducing deep and bottom waters in a world ocean model. *Journal of Physical*
427 *Oceanography*, 32(4), 1209-1227. [https://doi.org/10.1175/1520-](https://doi.org/10.1175/1520-0485(2002)032%3C1209:EOBBLP%3E2.0.CO;2)
428 [0485\(2002\)032%3C1209:EOBBLP%3E2.0.CO;2](https://doi.org/10.1175/1520-0485(2002)032%3C1209:EOBBLP%3E2.0.CO;2)
- 429 25. Nakazato, M., Kido, S., & Tozuka, T. (2021). Mechanisms of asymmetry in sea surface
430 temperature anomalies associated with the Indian Ocean Dipole revealed by closed heat
431 budget. *Scientific Reports*, 11(1), 22546. <https://doi.org/10.1038/s41598-021-01619-2>
- 432 26. Pujol, M. I., Faugère, Y., Taburet, G., Dupuy, S., Pelloquin, C., Ablain, M., & Picot, N.
433 (2016). DUACS DT2014: the new multi-mission altimeter data set reprocessed over 20
434 years. *Ocean Science*, 12(5), 1067-1090. <https://doi.org/10.5194/os-12-1067-2016>.
- 435 27. Ridderinkhof, H., Van der Werf, P. M., Ullgren, J. E., Van Aken, H. M., Van Leeuwen, P. J.,
436 & de Ruijter, W. P. M. (2010). Seasonal and interannual variability in the Mozambique
437 Channel from moored current observations. *Journal of Geophysical Research:*
438 *Oceans*, 115(C6). <https://doi.org/10.1029/2009JC005619>
- 439 28. Saji, N. H., Goswami, B. N., Vinayachandran, P. N., & Yamagata, T. (1999). A dipole mode
440 in the tropical Indian Ocean. *Nature*, 401(6751), 360-363. <https://doi.org/10.1038/43854>
- 441 29. Suresh, I., Vialard, J., Lengaigne, M., Han, W., McCreary, J., Durand, F., & Muraleedharan,
442 P. M. (2013). Origins of wind-driven intraseasonal sea level variations in the North Indian
443 Ocean coastal waveguide. *Geophysical Research Letters*, 40(21), 5740-5744.
444 <https://doi.org/10.1002/2013GL058312>
- 445 30. Suresh, I., Vialard, J., Izumo, T., Lengaigne, M., Han, W., McCreary, J., & Muraleedharan,
446 P. M. (2016). Dominant role of winds near Sri Lanka in driving seasonal sea level variations
447 along the west coast of India. *Geophysical Research Letters*, 43(13), 7028-7035.
448 <https://doi.org/10.1002/2016GL069976>.
- 449 31. Suresh, I., Vialard, J., Lengaigne, M., Izumo, T., Parvathi, V., & Muraleedharan, P. M.
450 (2018). Sea level interannual variability along the west coast of India. *Geophysical Research*
451 *Letters*, 45(22), 12-440. <https://doi.org/10.1029/2018GL080972>
- 452 32. Tanizaki, C., Tozuka, T., Doi, T., & Yamagata, T. (2017). Relative importance of the

- 453 processes contributing to the development of SST anomalies in the eastern pole of the Indian
454 Ocean Dipole and its implication for predictability. *Climate Dynamics*, 49, 1289-1304.
455 <https://doi.org/10.1007/s00382-016-3382-2>
- 456 33. Tatebe, H., Ogura, T., Nitta, T., Komuro, Y., Ogochi, K., Takemura, T., et al. (2019).
457 Description and basic evaluation of simulated mean state, internal variability, and climate
458 sensitivity in MIROC6. *Geoscientific Model Development*, 12(7), 2727-2765.
459 <https://doi.org/10.5194/gmd-12-2727-2019>
- 460 34. Tsujino, H., Urakawa, L. S., Griffies, S. M., Danabasoglu, G., Adcroft, A. J., Amaral, A. E.,
461 et al. (2020). Evaluation of global ocean–sea-ice model simulations based on the
462 experimental protocols of the Ocean Model Intercomparison Project phase 2 (OMIP-
463 2). *Geoscientific Model Development*, 13(8), 3643-3708. [https://doi.org/10.5194/gmd-13-](https://doi.org/10.5194/gmd-13-3643-2020)
464 [3643-2020](https://doi.org/10.5194/gmd-13-3643-2020)
- 465 35. Varna, M., Jithin, A. K., & Francis, P. A. (2023). Characteristics and dynamics of mesoscale
466 eddies in the eastern Arabian Sea. *Deep Sea Research Part II: Topical Studies in*
467 *Oceanography*, 207, 105218. <https://doi.org/10.1016/j.dsr2.2022.105218>
- 468 36. Vinayachandran, P. N., Shankar, D., Kurian, J., Durand, F., & Shenoi, S. S. C. (2007).
469 Arabian Sea mini warm pool and the monsoon onset vortex. *Current Science*, 93(2), 203–
470 214. <http://www.jstor.org/stable/24099306>
- 471 37. Wang, B., & Xie, X. (1997). A model for the boreal summer intraseasonal
472 oscillation. *Journal of the Atmospheric Sciences*, 54(1), 72-86. [https://doi.org/10.1175/1520-](https://doi.org/10.1175/1520-0469(1997)054%3C0072:AMFTBS%3E2.0.CO;2)
473 [0469\(1997\)054%3C0072:AMFTBS%3E2.0.CO;2](https://doi.org/10.1175/1520-0469(1997)054%3C0072:AMFTBS%3E2.0.CO;2)
- 474 38. Wyrtki, K. (1973). An equatorial jet in the Indian Ocean. *Science*, 181(4096), 262-264.
475 <https://doi.org/10.1126/science.181.4096.262>
- 476 39. Yoshida, K. (1960). A Theory of the Cromwell Current (the Equatorial Undercurrent) and of
477 the Equatorial Upwelling. *Journal of the Oceanographical Society of Japan*, 15(4), 159-170.
478 <https://doi.org/10.5928/kaiyou1942.15.159>
- 479 40. Zweng, M. M., Seidov, D., Boyer, T. P., Locarnini, M., Garcia, H. E., Mishonov, A. V., et al.
480 (2019). World ocean atlas 2018, volume 2: Salinity. NOAA Atlas NESDIS 82,
481 50pp. <https://archimer.ifremer.fr/doc/00651/76339/>